

## Numerical Study of the Energy Absorption Performance of 3D Printed Sandwich Structures

Quirino Estrada<sup>1\*</sup>, Jarosław Zubrzycki<sup>2</sup>, Elva Reynoso<sup>1</sup>, Dariusz Szwedowicz<sup>3 †</sup>,  
Alejandro Rodriguez-Mendez<sup>4</sup>, Magdalena Marchewka<sup>2</sup>, Julio Vergara<sup>5</sup>,  
Aztlán Bastarrachea<sup>6</sup>, Jesús Silva<sup>1</sup>

<sup>1</sup> Instituto de Ingeniería y Tecnología, Universidad Autónoma de Ciudad Juárez (UACJ), Ciudad Juárez, Chihuahua, México

<sup>2</sup> Mechanical Engineering Faculty, Lublin University of Technology, ul. Nadbystrzycka 38D, 20-618 Lublin, Poland

<sup>3</sup> Centro Nacional de Investigación y Desarrollo Tecnológico/TecNM, Cuernavaca, Morelos, México, Mexico

<sup>4</sup> Tecnológico Nacional de México campus Ciudad Guzmán, Ciudad Guzmán, Jalisco, Mexico

<sup>5</sup> Unidad Profesional Interdisciplinaria de Ingeniería, Campus Palenque (UPIIP)/IPN, Palenque, Chiapas, Mexico

<sup>6</sup> Departamento de Ciencias Básicas, Tecnológico Nacional de México campus Ciudad Juárez, Ciudad Juárez, Chihuahua, Mexico

\* Corresponding author's email: [quirino.estrada@uacj.mx](mailto:quirino.estrada@uacj.mx)

### ABSTRACT

Nowadays, Fused Deposition Modeling (FDM) is a powerful tool for manufacturing complex components, due to its customizability, low cost, accessibility, and fast prototyping time. It is an alternative for creating thin-walled structures, as it allows for novel designs. This article focuses on the design and numerical evaluation of 3D printed sandwich structures for energy absorption applications. For this purpose, five structures of Acrylonitrile Butadiene Styrene (ABS) were designed. To ensure optimal performance, the 3D printing parameters were optimized based on the corresponding literature. The structures had cores based on polygonal and cell arrangements. The effects of cross-section and mass on energy absorption were analyzed, and parameters such as energy absorption, peak load, mean force, and crush force efficiency (CFE) were determined during the study. The structures were assessed by out-of-plane compression tests. The numerical analysis was executed using Abaqus finite element software. Results showed that the energy absorption performance is primarily determined by the geometry and density of the structures. The best performance was found for a circular cellular structure, with a CFE of 0.884.

**Keywords:** sandwich structures, crashworthiness, 3D printed, energy absorption.

### INTRODUCTION

Since the emergence of Fused Deposition Modeling (FDM) for rapid prototyping in the 1980s, its use in engineering has increased exponentially [1–3]. 3D printers build components by adding material layer by layer [4–5], using a thermoplastic filament such as Acrylonitrile Butadiene Styrene (ABS) or Polylactic Acid (PLA) extruded and deposited by a heated nozzle [6]. 3D printing has many advantages, such as low

cost, material savings, customizability, and decreased manufacturing time among others. As such, 3D printing has been proposed for a variety of applications, including mechanical components [7–8], medical applications [9–11], and architected materials [12–13]. One of the most relevant applications today is the fabrication of energy absorption structures for crashworthiness [14–15]. Several studies have been conducted to analyze the mechanical properties of 3D printed components, particularly their energy absorption

and resistance performance [16–17]. In a study conducted by Andrew et al. [18], the energy absorption performance of 3D printed CF/PEEK composite structures was analyzed. The experimental investigation included structures with hexagonal, chiral, and re-entrant lattice shapes. The study demonstrated the effectiveness of these 3D composite structures, as they offered advantages such as lightweight design and high performance. Similarly, Sankineni [19] evaluated the energy absorption capacities of 3D structures printed with PLA material. The analysis focused on cellular and triply periodic minimal surface (TPMS) structures. Among the TPMS structures, the deformed Gyroid structure exhibited superior energy absorption capacity, withstanding strains of up to 11.6%. In another experimental program, Zubrzycki et al. [20] evaluated the influence of 3D printing parameters, using the FDM method, on the mechanical properties of structural components. This study enabled the determination of the optimal printing parameters based on the forecasted load requirements for the components. Sarvestani et al. [21] developed and analyzed the energy absorption performance of 3D printed architected polymeric sandwich panels. They focused on the core of the structures, considering topology and density, and proposed alternative cellular core architectures such as auxetic, rectangular, and hexagonal geometries. The structures were evaluated via low-velocity impact tests. The best crashworthiness performance was found for the auxetic sandwich panel. Menegozzo et al. [22] proposed a novel honeycomb cell geometry design, consisting of internal diagonal walls to support the external walls. The honeycombs were evaluated through quasistatic axial and lateral compressive load, using both experimental and numerical methods. The specimens were manufactured with ABS thermoplastic material. Compared to a hexagonal structure as a control, a 15% increase in energy absorption was calculated. Bolan et al. [23] evaluated the energy absorption of 3D-Printed Polymeric Octet-Truss Lattice Structures, fabricated from two different acrylate resins and cured under UV lighting. Quasi-static compression tests were conducted and the effect of strut length, radius, material, and density was confirmed to determine the failure mode. A semi-empirical model for predicting energy absorption was also proposed. 3D printing technology has emerged as a powerful tool for designing innovative cellular energy absorption structures, offering

the ability to explore complex and unique topologies. As mentioned above, research on 3D printed structures has largely focused on the experimental, numerical, and theoretical assessment of printing parameters and materials. Unfortunately, there is a scarcity of studies examining the impact of cellular structure topology and mass on out-of-plane load behavior. Consequently, there is a distinct need to expand the body of knowledge in this area since the majority of the reported research focuses on flexion, lateral, and in-plane compression loading conditions. Thus, the objective of this work, therefore, is to design and evaluate five novel sandwich structures featuring triangular, square, and circular geometries. Two types of configurations are investigated. The first type involves single geometries while the second type is called cellular arrangements, which consist of individual shapes connected by ribs. The direct effect of the ribs was also analyzed. These structures were built using ABS material, and their performance will be assessed numerically through out-of-plane quasi-static compression tests. By emphasizing the geometric aspects and mass performance of the structures, this study aims to furnish designers with valuable findings, beyond the scope of printing parameters, to inform the creation of energy absorption structures.

## RESEARCH AND METHODS

### Crashworthiness metrics

Crashworthiness is the capacity of a structure to resist impact forces while maintaining the integrity of the passengers during a collision. This is achieved through the controlled deformation of the structure. Several parameters have been proposed to evaluate crashworthiness performance, the most important of which are listed in Table 1, with  $F$  denoting the axial force,  $\delta$  the displacement, and  $m$  the mass [24].

### Material characterization of acrylonitrile butadiene styrene

The sandwich structures were printed with ABS. The mechanical properties of ABS were studied using an ASTM D638 tensile test designed for plastic materials. Type I tensile samples were printed on a Zortrax® M200 with an infill of 100% (see Figure 1). To understand the

**Table 1.** Relevant crashworthiness parameters [24]

Peak load [ $P_{max}$ ] kN	Mean Force [ $P_m$ ] kN	Energy absorbed [ $E_a$ ] kJ	Crush force efficiency [CFE]	Specific energy absorption [SEA]
Obtained from curve	$P_m = \frac{E_a}{\delta}$	$E_a = \int_0^{\delta} F \cdot d\delta$	$CFE = \frac{P_m}{P_{max}}$	$SEA = \frac{E_a}{m}$

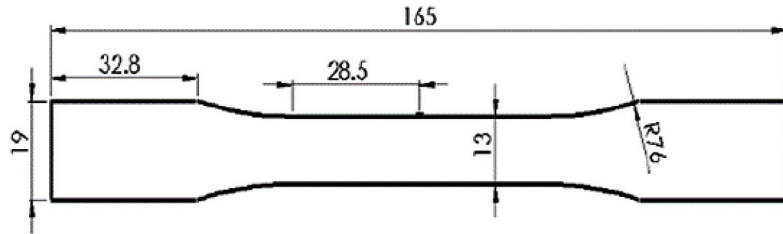


**Fig. 1.** Geometric characteristics of a type I sample for an ASTM D638 test; units in mm [25]



**Fig. 2.** ABS samples printed with printing angle of 0°, 45° and 90°

mechanical behavior of the samples in relation to the printing orientation angle, samples were printed at 0°, 45°, and 90°, as shown in Figure 2.

The tensile test was conducted on a Shimadzu AG-X Plus 100kN universal test machine at a

speed of 5 mm/min. The deformation was measured using an Epsilon 3542-050M-050-ST extensometer. Details of the experimental setup and samples are shown in Figure 3. Three tests were conducted for each printing angle to ensure the accuracy of the results. The stress versus deformation curves, as depicted in Figure 4, demonstrate the influence of the printing angle on the mechanical response of the samples, consistent with reported in the literature [20]. As anticipated, the sample printed at a 0° angle exhibited the lowest strength performance. Conversely, the samples printed at 45° and 90° angles exhibited superior strength performance. It is worth noting, however, that the samples printed at a 90° angle displayed a greater strain at the beginning of the tensile test. From these curves, a Young modulus

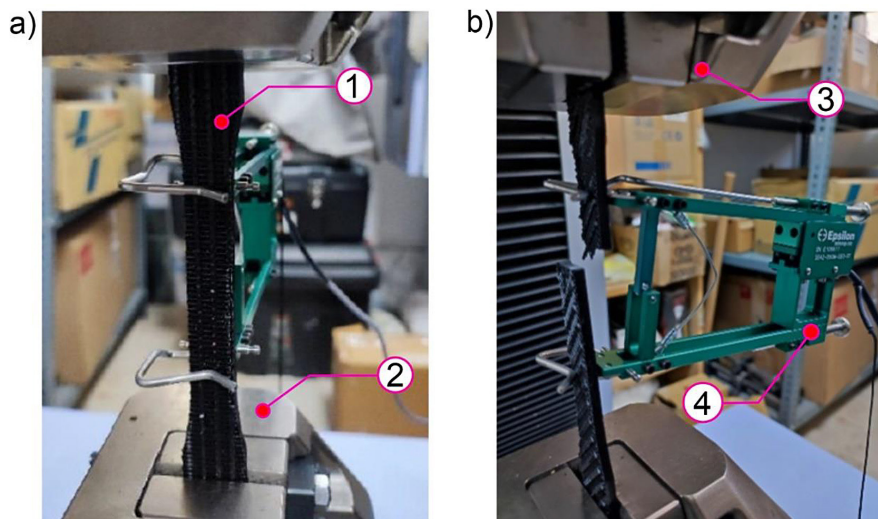


**Fig. 3.** (a) Before and (b) after images of the ASTM D638 Tensile test, where the numbers in the image indicate: 1-Printed sample, 2-lower jaw, 3-upper jaw and 4-extensometer

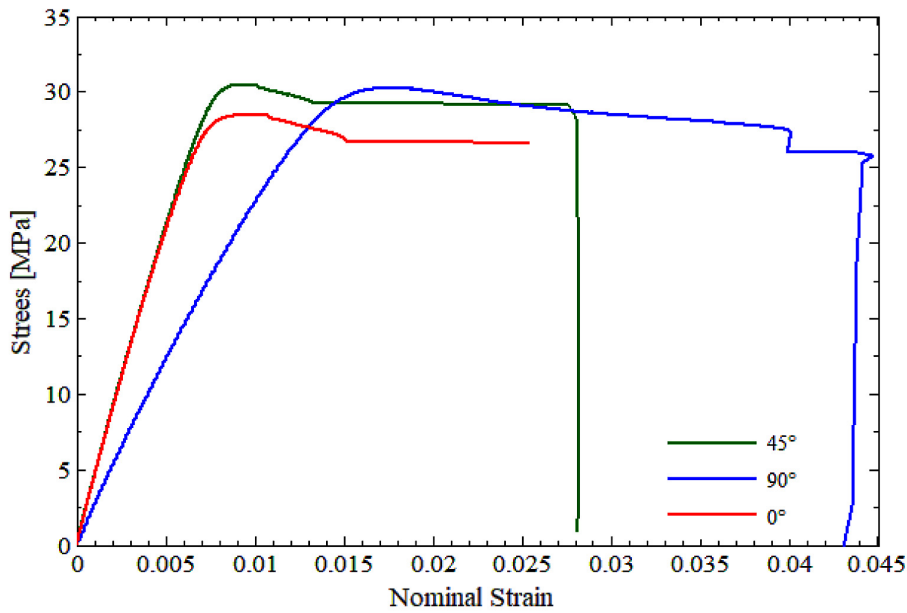


Fig. 4. Stress vs strain curves for the samples made of ABS material with different printing angles

of 2451 MPa and a yield stress of 29.16 MPa were calculated, which are consistent with literature data [26]. Since similar maximum strengths were computed for samples printed at 45° and 90°, these curves were used in the next section.

### First numerical model

In order to guarantee the feasibility of numerical techniques, a tensile test discrete model was developed in Abaqus/Explicit software. The sample was modeled with S4R elements, with elastoplastic properties for ABS material, a Young modulus of 2451 MPa, a yield stress of 29.16 MPa, a Poisson coefficient of 0.38, and a density of 1024 kg/m<sup>3</sup> (see Section 3). Fixed conditions were imposed on the left end, while a velocity condition was applied to the nodes on the right end. The strain was determined by analyzing the X1 and X2 node references

shown in Figure 5, which are separated by 50 mm, as indicated in [25]. Details of the discrete model are presented in Figure 5. A comparison of numerical and experimental results for the strain vs. stress curves is shown in Figure 6. As can be seen, the discrete model accurately reproduces both the quantitative and qualitative mechanical response of the sample, with a maximum resistance close to 29 MPa. The difference between the models is less than 3%. The numerical model is thus corroborated and it is possible to continue with the analysis of the ABS printed sandwich structures.

### Numerical analysis of the 3D printed sandwich structures

The main purpose of this article is to evaluate the energy absorption performance of new 3D printed sandwich structures. Five structures were

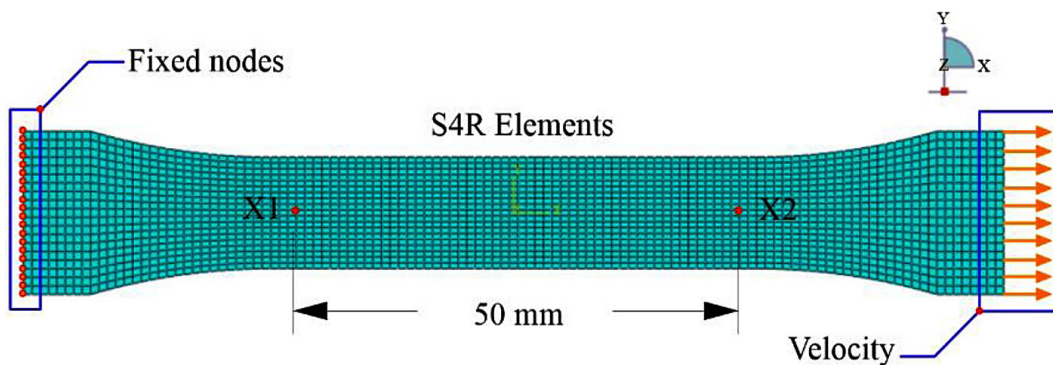


Fig. 5 Coordinate system and discrete model used for the tensile test

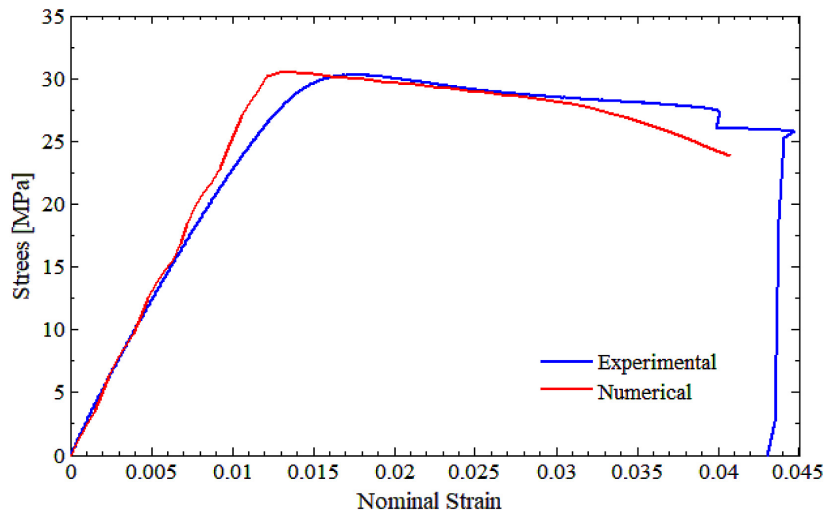


Fig. 6. Comparison of stress vs strain curves between numerical and experimental tests

designed based on square, triangular, and circular patterns. The structures consist of a core structure encapsulated by two face-sheets (skins), with The core dimensions are 70 mm in length (L) and width (W), with a height (H) of 50 mm. The skins, on the other hand, have a length and width of 80 mm and a thickness of 2 mm. All structures were given mechanical properties for Acrylonitrile Butadiene Styrene material (see Section 3). Table 2 presents the details of the structures with the top skin hidden to show the geometrical patterns. The structures were numerically evaluated via quasi-static out-of-plane compression tests at a speed of 6 mm/min. The out-of-plane refers to extrusion-direction. The bottom skin was constrained in all directions, while the top skin was unconstrained only in the y-direction to allow for the compression of the structure. During the simulation, the core and skins were modeled with shell element type S4R, and the plates were considered as rigid bodies with R3D4 elements. A friction coefficient of 0.15 was used for the contact interaction between the skins and the compression plates. To avoid condensation and to capture the effect of the core geometry, a crushing length of 33 mm

was established. Lastly, an element size of 2 mm was determined based on a mesh convergence analysis. The discrete model is shown in Figure 7.

## RESULTS AND DISCUSSION

The mechanical behavior of the sandwich structures was determined through analysis of force displacement curves obtained from compression tests. Figure 8 shows that the geometry of the cell had a significant effect, resulting in different qualitative and quantitative behaviors. The sandwich structures can be divided into two groups based on geometric arrangement: the first group consists of cores based on polygonal shapes (SSQ, SS45, and SRB), while the second group consists of structures with cores formed by a cellular arrangement, such as SCC and SSC. In the case of the first group, the qualitative behavior was characterized by a rapid increase in force at the beginning of the compression test, followed by a sudden decrease until reaching a stable behavior. This behavior is typical and it has been reported for polygonal structures under

Table 2. Geometric characteristics of the 3D printed sandwich structures, units in mm

Specimen code	Base	Thickness (t)	Mass (gr)
SSQ	Square	0.5	28.1
SS45	Square	0.5	45.8
SRB	Rhomboidal	0.5	36.1
SCC	Circular	0.5	50.6
SSC	Square	0.5	60.1

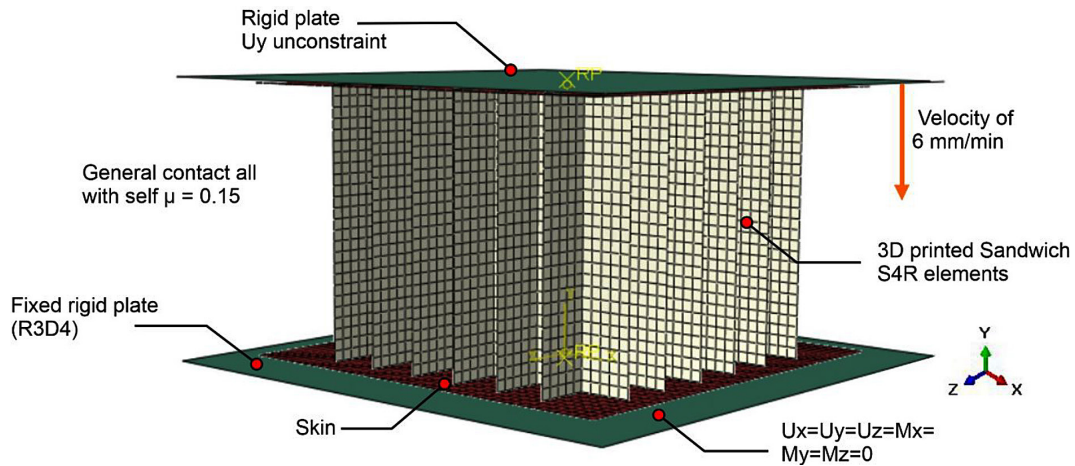


Fig. 7. Discrete model for the compression test of 3D printed sandwich structures (specimen SSQ shown for reference)

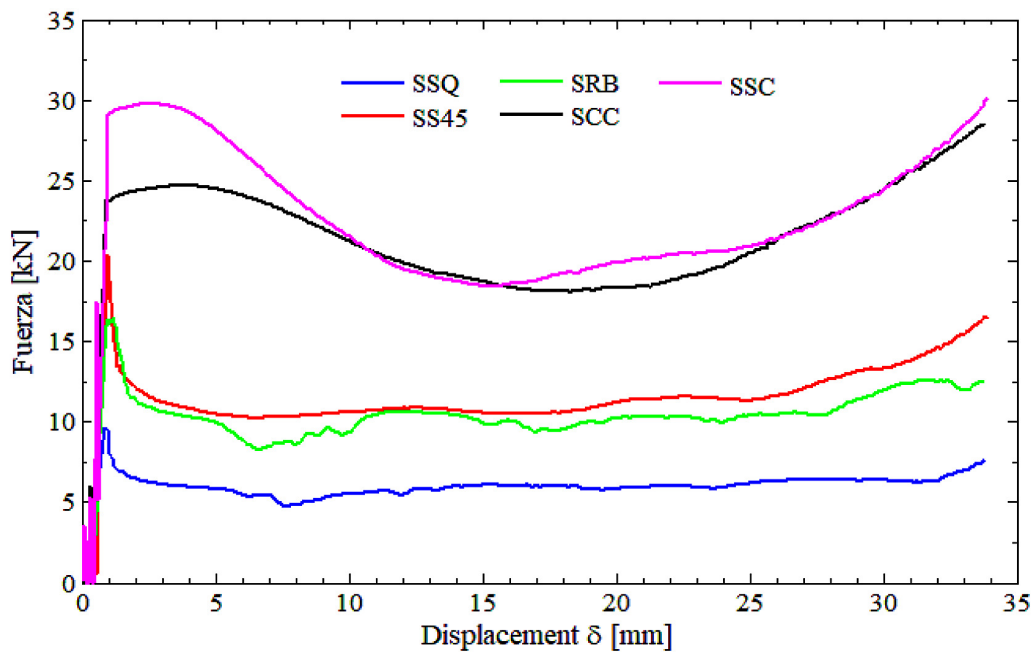


Fig. 8. Compression force vs displacement curves for 3D printed sandwich structures

out-of-plane compression loads [18, 28]. Conversely, structures SCC and SSC exhibited a gentle decrease in force during the first 10 mm of displacement. During the crushing process, the force showed a wave-like behavior without reaching stabilization. The cellular cores exhibited higher strength than the polygonal cores, as evidenced by the peak load ( $P_{max}$ ) values ranging from 9-30 kN. The highest resistance was observed in structure SCC, which had a  $P_{max}$  value close to 30 kN. In all cases, a densification phase was observed at the end of the test. The densification phase occurs when a displacement of 25 mm is reached. This phenomenon

can be attributed to a higher interaction among the walls, leading to an increase in the crushing force, as explained in [28].

The collapse mode determines the mechanical response and energy absorption capacity of the structures. The stiffness provided by the cell pattern determines the generation of static and dynamic yield hinge lines during the compression test. In the first group, progressive deformation of the cells is observed (see Figure 9), with visible buckle effects, especially in structures with a rhomboidal pattern (SRB), as evidenced by the large difference between  $P_{max}$  and  $P_m$  in Figure 8. Structures with cell arrangement (SCC and

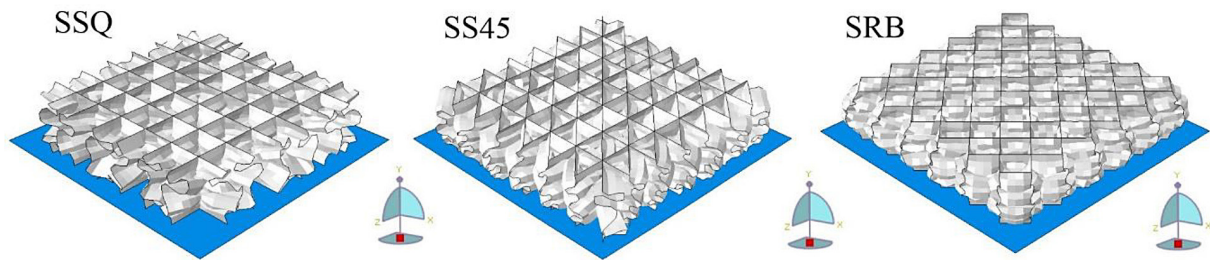


Fig. 9. Final deformation state for the 3D sandwich structures made of polygonal cores

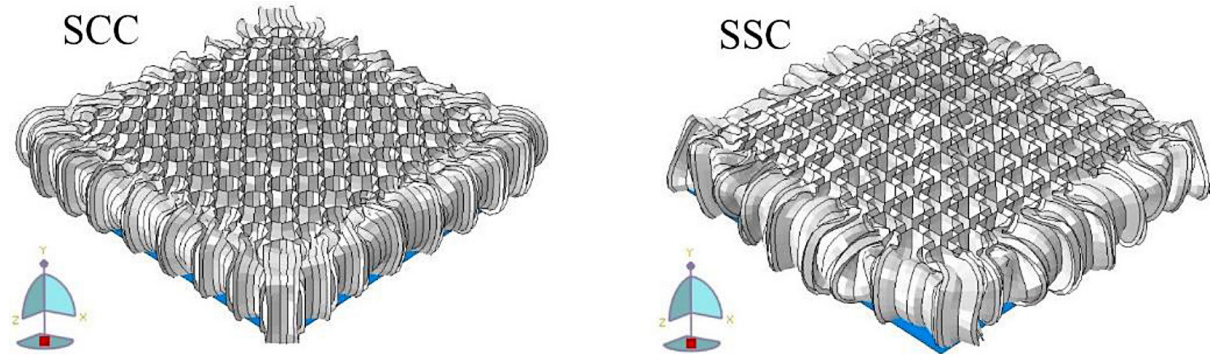


Fig. 10. Final deformation state for the 3D sandwich structures made of cellular arrangements

SSC) exhibit better stress distribution, thanks to the ribs acting as joint elements between circular and square shapes. This improved stress distribution increasing the strength of the structures. New hinge lines were formed in these elements, as shown in Figure 10. Cells located around the periphery of the sandwiches experienced higher deformation as they are not encapsulated. This behavior is expected due to the lack of constraints on the outer elements, allowing them to rotate around the x-axis. This phenomenon has been previously observed and documented in the literature [27]. In Figures 9 and 10 the top skins were hidden to easily observe the pattern deformation of the cores. For the quantitative analysis of the sandwich structures, the most representative energy absorption indicators were calculated using the mathematical expressions presented in Table

1. The results are presented in Table 3. Structures with cellular arrangements (SCC and SSC) showed better mechanical response compared to structures based on polygonal forms without ribs. The structure SSC exhibited the maximum strength resistance with a  $P_{max}$  value of 29.77 kN. This represents a 32% improvement compared to the weakest structure SSQ (structure with typical grid core) with a computed value of 9.60 kN. The improved performance of the SSC structure can be attributed to better stabilization of the core under load, as evidenced by the lower mean force ( $P_m$ ) value of 6.09 kN, indicating the low stiffness of the square pattern in the SSQ structure. Energy absorption ( $E_a$ ) is an important parameter as it considers both elastic and plastic deformations.  $E_a$  values ranging from 0.201 kJ to 0.761 kJ were obtained. The structure with the best  $E_a$

Table 3. Summary of relevant energy absorption indicators calculated for ABS sandwich structures

Specimen code	Peak load $P_{max}$ (kN)	Mean crushing force $P_m$ (kN)	Energy absorption $E_a$ (kJ)	Specific energy absorption SEA (J/gr)	Crushing force Efficiency CFE
SSQ	9.60	6.09	0.201	7.153	0.634
SS45	20.34	11.75	0.388	8.471	0.577
SRB	16.45	10.57	0.349	9.667	0.642
SCC	24.67	21.81	0.720	14.229	0.884
SSC	29.77	23.06	0.761	12.662	0.774

performance of 10.76 kJ was the one with a circular cellular arrangement (SSC), representing a 278% improvement compared to the lowest  $E_a$  value obtained. Considering the different masses of the structures, the specific energy absorption (SEA) was calculated to identify the best ratio between mass and  $E_a$ . The structure with a circular cellular arrangement (SSC) exhibited the highest SEA value of 14.229 J/g. In general, cellular arrangements tend to exhibit better  $E_a$  performance compared to typical rectangular structures. This is attributed to the high-density that can be achieved at the core, which is in agreement with the findings described in [21].

As mentioned earlier, structures with square cellular arrangements exhibit higher resistance ( $P_{max}$ ) and  $E_a$ . However, this does not necessarily mean they have the best crashworthiness behavior. To evaluate this, the crush force efficiency (CFE) was calculated. The cellular arrangements (SCC and SSC) showed better performance than their polygonal counterparts. CFE values ranging from 0.774 to 0.884 were obtained. The best CFE performance, with a value of 0.884, was achieved by the circular cellular arrangement (SCC). This corresponds to a 53% increase compared to the typical sandwich structure (SS45). Physically, at the beginning of the compression test, the circular geometry allows for a better distribution of stress along the rib joints. The circular shape, reinforced by ribs, provides greater stability to the structure, resulting in a larger area under the stress-strain curve. At this stage, a greater contact interaction between the cells and join-plates takes place, effectively minimizing the buckling effect. Additionally, due to the high-density nature of cellular structures, the core exhibits less porosity. This characteristic contributes to achieving a higher crushing force during the compression test. Based on this, sandwich structures with circular cellular arrangements are recommended for crashworthiness applications. There are many advantages associated with these structures, including excellent energy absorption capacity, low weight, relative low peak load with the plates acting as joint connections [21].

## CONCLUSIONS

In this article, we analyzed the energy absorption and strength of 3D sandwich structures made with ABS using the finite element

method. We assessed five structures with cores based on polygonal and cellular arrangements through compression tests. Based on our numerical simulations, we draw the following conclusions. The fused deposition method (3D printing) is a powerful tool for designing thin-walled structures. It allows for the creation of complex geometries that are lightweight, yet possess acceptable strength and are cost-effective. As demonstrated in Section 3, the printing angle has a significant impact on the mechanical response of the printed components. Therefore, this parameter should be determined based on the specific application of the sandwich structures, such as axial or bending load. When it comes to sandwich structures, cellular cores exhibited better resistance compared to polygonal cores without ribs. This resulted in improved load carrying capacity. Physically, the ribs increased the stability of the structure. Moreover, cellular structures exhibit larger densities, so more interaction at the core walls is achieved. The highest resistance, equal to 29.77 kN, was calculated for the SSC structure. This represents an increase of 32% compared to the typical grid core (SSQ).

The energy absorption of the structures depends on the geometry of the core. Cellular arrangements showed an increase in this parameter of 278% compared to the SSQ structure (single shape). The ribs in the cellular cores contributed to better structural stability and controlled deformation. At this point, the ribs played a significant role in preventing buckling phenomena and promoting the formation of a greater number of hinge lines. The analysis of specific energy absorption (SEA) revealed a heavier structure does not necessarily mean better performance in terms of  $E_a$ . The best SEA value of 14.229 kJ was calculated for the circular cellular arrangement (SCC). In terms of crush force efficiency (CFE), cellular arrangement cores (SSC and SCC) demonstrated improvements ranging from 34% to 53% compared to the lowest CFE value of 0.577, which was calculated for the SS45 sandwich structure. This meant a low value of  $P_{max}$  with an acceptable energy absorption. Lastly, considering the high CFE value of 0.884 exhibited by the circular cellular core (SCC), this particular geometry pattern is highly recommended for applications requiring energy absorption. It combines acceptable resistance with low weight.

## Acknowledgements

This work is dedicated to the memory of Dr. Dariusz Szwedowicz. Those of us who worked with him, friends, colleagues, and students, express our gratitude and recognition for his invaluable human qualities, as well as for his contribution in the field of mechanical design and Mechanical Engineering for over 30 years in Mexico. As a mentor to researchers, his legacy lives on. Rest in peace, dear and beloved Professor.

## REFERENCES

1. Spoerk M., Savandaiah C., Arbeiter F., Sapkota J., Holzer C. Optimization of mechanical properties of glass-spheres-filled polypropylene composites for extrusion-based additive manufacturing. *Polymer Composites Journal* 2019, 40(2), 638–651.
2. Ngo T. D., Kashani A., Imbalzano G., Nguyen K. T., Hui D. Additive manufacturing (3D printing): A review of materials, methods, applications and challenges. *Composites; Part B: Engineering Journal* 2018, 143: 172–196.
3. Kristiawan R. B., Imaduddin F., Ariawan D., Ubaidillah, Arifin Z. A review on the fused deposition modeling (FDM) 3D printing: Filament processing, materials, and printing parameters. *Open Engineering Journal* 2021, 11(1), 639–649.
4. Dawoud M., Taha I., Ebeid S. J. Mechanical behaviour of ABS: An experimental study using FDM and injection moulding techniques. *Journal of Manufacturing Processes* 2016; 21: 39–45.
5. Pham D. T., Gault R. S. A comparison of rapid prototyping technologies. *International Journal of machine tools and manufacture* 1998, 38(10-11), 1257–1287.
6. Rodríguez-Panes A., Claver J., Camacho A. M. The influence of manufacturing parameters on the mechanical behaviour of PLA and ABS pieces manufactured by FDM: A comparative analysis. *Materials Journal* 2018, 11(8), 1333.
7. Bastarrechea A., Estrada Q., Zubrzycki J., Torres-Argüelles V., Reynoso E., Rodríguez-Mendez A., Coutiño E. Mechanical design of a low-cost ABS hand prosthesis using the finite element method. *Journal of Physics: Conference Series* 2021, 1736 (1), 012039.
8. Yadav D. K., Srivastava R., Dev S. Design & fabrication of ABS part by FDM for automobile application. *Materials Today: Proceedings Journal* 2020, 26: 2089–2093.
9. Zhao F., Li D., Jin Z. Preliminary Investigation of Poly-Ether-Ether-Ketone Based on Fused Deposition Modeling for Medical Applications. *Materials Journal* 2018, 11: 288.
10. Haryńska A., Kucinska-Lipka J., Sulowska A., Gubanska I., Kostrzewa M., Janik H. Medical-grade PCL based polyurethane system for FDM 3D printing—characterization and fabrication. *Materials Journal* 2019, 12(6), 887.
11. Pu'ad N. M., Haq R. A., Noh H. M., Abdullah H. Z., Idris M. I., Lee T. C. Review on the fabrication of fused deposition modelling (FDM) composite filament for biomedical applications. *Materials Today: Proceedings Journal* 2020, 29: 228–232.
12. Mercado-Colmenero J. M., La Rubia M. D., Mata-Garcia E., Rodriguez-Santiago M., Martin-Doñate C. Experimental and numerical analysis for the mechanical characterization of pet polymers manufactured with fdm technology under pure uniaxial compression stress states for architectural applications. *Polymers Journal* 2020, 12(10), 2202.
13. Diaz-Perete D., Mercado-Colmenero J.M., Valderama-Zafra J.M., Martin-Doñate C. New Procedure for BIM Characterization of Architectural Models Manufactured Using Fused Deposition Modeling and Plastic Materials in 4.0 Advanced Construction Environments. *Polymers Journal* 2020, 12: 1498.
14. Silva R. D. C., Castro G. M., Oliveira A. B. D. S., Brasil A. C., Luz S. M. Crashworthiness performance of hybrid energy absorbers using PET-G honeycomb structure. *Mechanics Based Design of Structures and Machines Journal* 2022, 1–26.
15. Basurto-Vázquez O., Sánchez-Rodríguez E. P., McShane G. J., Medina, D. I. Load distribution on PET-G 3D prints of honeycomb cellular structures under compression load. *Polymers Journal* 2021, 13(12), 1983.
16. Bodaghi M., Serjouei A., Zolfagharian A., Fotouhi M., Rahman H., Durand D. Reversible energy absorbing meta-sandwiches by FDM 4D printing. *International Journal of Mechanical Sciences* 2020; 173: 105451.
17. Namvar N., Zolfagharian A., Vakili-Tahami F., Bodaghi M. Reversible energy absorption of elastoplastic auxetic, hexagonal, and AuxHex structures fabricated by FDM 4D printing. *Smart Materials and Structures Journal* 2022; 31(5): 055021.
18. Andrew J. J., Alhashmi H., Schiffer A., Kumar S., Deshpande V. S. Energy absorption and self-sensing performance of 3D printed CF/PEEK cellular composites. *Materials & Design Journal* 2021, 208: 109863.
19. Sankineni R., Ravi Kumar Y. Evaluation of energy absorption capabilities and mechanical properties in FDM printed PLA TPMS structures. *Proceedings of the Institution of Mechanical Engineers, Part C: Journal of Mechanical Engineering Science* 2022, 236(7), 3558–3577.

20. Zubrzycki J., Estrada Q., Staniszewski M., Marchewka M. Influence of 3D printing parameters by FDM method on the mechanical properties of manufactured parts. *Advances in Science and Technology Research Journal* 2022, 16(5), 52-63.
21. Sarvestani H. Y., Akbarzadeh A. H., Niknam H., Hermenean K. 3D printed architected polymeric sandwich panels: Energy absorption and structural performance. *Composite Structures Journal* 2018, 200: 886–909.
22. Menegozzo M., Cecchini A., Just-Agosto F. A., Serrano Acevedo D., Flores Velez O. J., Acevedo-Figueroa I., De Jesús Ruiz J. A 3D-Printed Honeycomb Cell Geometry Design with Enhanced Energy Absorption under Axial and Lateral Quasi-Static Compression Loads. *Applied Mechanics Journal* 2022, 3(1), 296–312.
23. Bolan M., Dean M., Bardelcik A. The Energy Absorption Behavior of 3D-Printed Polymeric Octet-Truss Lattice Structures of Varying Strut Length and Radius. *Polymers Journal* 2023, 15(3): 713.
24. Estrada, Q., Reynoso, E., Szwedowicz, D., Rodriguez-Mendez, A., Coutiño, E., De la Mora, T., & Torres, C. Bending crashworthiness of bionic thin-walled structures inspired by sugar cane stalks. *Journal of Physics: Conference Series*, 2412(1), #012003.
25. ASTM D 638–99, 1999, Standard Test Method for Tensile Strength of Plastics. *Annual Book of ASTM Standards*, ASTM International, West Conshohocken, PA.
26. Jones G., Stopforth R. Mechanical design and development of the touch hand ii prosthetic hand. *RD J. South African Inst. Mech. Eng Journal* 2016, 32: 23–34.
27. Kaveloglu, S., and Temiz, S. An experimental and finite element analysis of 3D printed honeycomb structures under axial compression. *Polymers and Polymer Composites* 2022, 30, 09673911221122333.
28. Zhang, Y., Zong, Z., Liu, Q., Ma, J., Wu, Y., & Li, Q. Static and dynamic crushing responses of CFRP sandwich panels filled with different reinforced materials. *Materials & Design* 2017, 117, 396–408.